Stereoscopic Particle Image Velocimetry: Application to a non-Newtonian Flow Field Generated by a Sedimenting Sphere

N.J. Lawson[+], J.A. Tatum, M.V. Finnis [+], G.M. Harrison

Department of Chemical Engineering, Clemson University, Clemson SC 29634, USA
[+]Cranfield University, College of Aeronautics, Cranfield MK43 0AL, UK

corresponding author: graham.harrison@ces.clemson.edu

ABSTRACT

The flow fields for a sphere sedimenting through a Newtonian and two non-Newtonian liquids near a wall in a square tank are characterized using angular stereoscopic 3D particle image velocimetry (PIV) experiments. The experiments use angular stereoscopic configurations with Scheimpflug tilt and shift arrangements and a pair of liquid correction prisms. Two image acquisition systems based on a pair of Kodak ES1.0 CCD's and New Wave Gemini pulsed Nd:YAG laser and a pair of NAC Hi-DCAM II CCD's and a Photonics Industries GM30-527-E laser are used to obtain the velocity field in two distinct planes defined by laser sheet orientations through the sphere centerline: parallel to and perpendicular to the adjacent planar vertical wall.

The sedimentation of a sphere through a fluid is a standard testbed problem in non-Newtonian fluid mechanics. The experimentally determined velocity fields may be compared with numerical simulations. In this work, the influence of an adjacent planar vertical wall, in addition to elastic and shear thinning effects, on the velocity field in the fluid surrounding the sphere is studied. Three different test fluids are employed: a Newtonian reference fluid, a constant shear viscosity (elastic) Boger fluid, and a shear thinning elastic fluid. All three fluids have similar zero shear viscosities. The Weissenberg and Reynolds numbers are manipulated by varying both the diameter and the composition of the ball. The effect of the distance from the vertical wall on the velocity field is investigated by dropping spheres one, two and three ball diameters from the wall. For all experiments, the terminal velocity is achieved before measurements begin.

From the experimental data, the influence of both the geometry and the fluid properties on the velocity flow field is evident. The basic shape of the wake upstream of the sphere is qualitatively different for the various fluids investigated. The motion perpendicular to the wall is strongly dependent on the initial distance that the sphere is dropped from the wall. The presence of the wall leads to fluid moving perpendicular to the wall and out towards the center of the tank. The magnitude and location of this motion is strongly fluid dependent. The location of the recirculation zones depends on both the fluid type and the Weissenberg number. A negative wake is observed in the experiments conducted with the shear-thinning fluid at high Weissenberg numbers. The Boger fluid exhibits little motion perpendicular to the wall, as the fluid motion is localized around the sphere due to the fluid elasticity.

1. INTRODUCTION

Significant challenges are presented to the computational fluid dynamicist when modeling the flow of a non-Newtonian fluid. In order to address some of these issues, a series of benchmark problems have been developed so that numerical developments are validated by experimental results [Hassager (1988)]. These test problems feature regions of shear flow as well as regions of extensional flow. One of these problems is that of a sphere sedimenting along the centerline of a cylindrical tank through a quiescent fluid. From a modeling perspective, particular challenges arise both in the numerical scheme employed and in the form of the constitutive equation that relates the stress to the velocity gradients in the flow. Given these issues concerning the development and use of appropriate constitutive equations, it is instructive to measure the experimental velocity flow field surrounding a sedimenting sphere and to compare this with the equivalent numerical prediction. Several different types of fluid have been employed in these experiments. Newtonian fluids adhere to Stokes' Law. Boger fluids are dilute polymer solutions that exhibit elastic effects while maintaining a constant shear viscosity. Shear-thinning elastic fluids are polymer solutions with a shear-rate dependent shear viscosity. Different constitutive equations must be used to effectively model each of these fluid types, both in simple shear flow and in the more complex extensional flows.

In most of the early experimental work in this field, investigators focused on measuring the drag coefficient as a function of the Reynolds number and the Weissenberg (or Deborah) number [e.g. see Tanner (1963), Chhabra et al (1980), Chmielowski et al (1990)]. These experiments focused on the steady state velocity of the sedimenting sphere. More recent work has focused on the measurement of the velocity field in the fluid generated by the sedimenting sphere. Both flow visualization and optical techniques, including laser Doppler anemometry (LDA) and particle image velocimetry (PIV) [Bush (1993), (1994), Arigo and McKinley (1998)], have been employed. Several interesting flow phenomena have been observed using these advanced techniques, including stagnation points in the flow and so-called negative wakes [Sigli and Coutanceau (1977), Arigo and McKinley (1998)]. These negative wakes, in which the fluid upstream of the sphere flows in the direction opposite to that of the sedimenting sphere, have been observed in those experiments with shear-thinning, elastic liquids.

The benchmark problem described above has in more recent studies been modified by allowing the sphere to sediment near a planar vertical wall. In this geometry, several other unique flow phenomena have been observed in experiments. Joseph *et al.* (1994) observed the sphere migrating either towards or away from the vertical plane depending on the type of fluid in which the sphere was dropped. In addition, Joseph et al. reported anomalous rotation, whereby the sphere rotates as if it were climbing, rather than falling down, near the wall. Subsequent investigations employing experimental visualization techniques as well as numerical simulations by both Becker *et al.* (1996) and Singh and Joseph (2000) have further explored the results from the initial flow visualization studies. Harrison *et al* (2001) experimentally investigated a sphere sedimenting near a planar wall using a 3-D stereoscopic PIV method. They measured all three components of the velocity in a plane parallel to the wall and through the centerline of the sphere. While sphere rotation and migration were not observed, significant fluid motion perpendicular to the wall was recorded, indicating how the flow field is impacted by the presence of the wall.

In the work presented here, an angular stereoscopic 3-D PIV system is used to study the flow fields around a sphere sedimenting through three different test fluids near a planar vertical wall. The fluids include a Newtonian reference fluid, a constant shear viscosity (elastic) Boger fluid, and a shear thinning elastic fluid that all have similar zero shear viscosities. The influence of the adjacent wall, in addition to elastic and shear thinning effects, on the velocity field in the fluid surrounding the sphere is investigated.

2. EXPERIMENTAL SET-UP

The following section describes the experimental PIV set-up and the fluids used for the PIV measurements.

2.1 Experimental Geometry

The test tank had dimensions 200mm (l) × 200mm (w) × 500mm (h). The 500mm height was chosen to ensure terminal velocity of the sphere was reached by the mid-height of the tank. In the results presented in this paper, the spheres were dropped at a distance of one ball diameter from one of the tank walls. Two

different orientations for the laser sheet were employed: (1) the laser sheet is oriented parallel to the wall and through the centerline of the sphere, and (2) the laser sheet is oriented perpendicular to the wall and through the centerline of the sphere. These orientations are shown in Figure 1a and 1b, respectively.

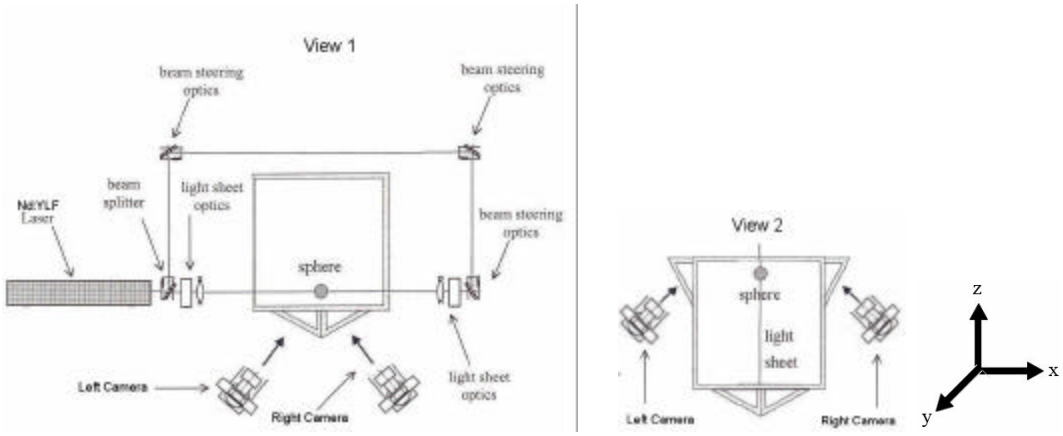

a) b)

Figure 1 – top view of experimental set-up. a) measurement plane parallel to near wall; b) measurement plane perpendicular to near wall.

2.2 Stereoscopic PIV Set-Up

The laser measurement technique particle image velocimetry (PIV) [Adrian, (1991)] is now increasingly being used in a stereoscopic configuration. Stereoscopic PIV allows the measurement of the 3D flow field about a selected measurement plane [Prasad (2000)].

Figure 1 shows the basic stereoscopic PIV set-up employed in this work. The system is based on an angular viewing arrangement with tilt and shift mounts to obtain the Scheimpflug condition. The angular Scheimpflug arrangement provides the best accuracy for a given camera semi-angle a [Prasad (2000)]. The camera semi-angle was set to between a = 15^o–25^o to provide optimum performance [Lawson and Wu (1997)] with an expected error ratio of around 3.5. Pairs of liquid correction prisms are mounted onto the tank to reduce image distortion [Prasad and Jensen (1995)]. The liquid prisms were filled with a near 50/50 water/glycerol solution and set at 15^o to correspond to with the minimum camera angle. The solution employed provides an acceptable refractive image match with the range of fluids used for the tests. Two sets of prisms were mounted onto the main test tank to allow the viewing of the object planes at both parallel and perpendicular planes to the tank wall (see Figure 1). All measurement planes were positioned below the mid-height of the tank to ensure terminal velocity was achieved. The acquisition process was triggered using a TTL pulse generated from a trigger box and a 1mW photodiode trigger laser. The trigger laser was placed in the path of the falling sphere and projected into the trigger box aperture. The acquisition point was also varied by introducing a delay between the trigger laser and PIV image acquisition sequence. This allowed the flow structure to be investigated both before and after the sphere.

The imaging system consisted of two independent PIV systems with ILA VidPIV software for data processing in each case. Two imaging systems were used due to equipment availability. The first imaging system was based on a pair of Kodak ES1.0 CCD's with a resolution of 1012 x 1024 pixels and a New Wave Gemini Nd:YAG pulsed laser system. Laser and camera triggering was obtained through the use of an ILA synchronization box. The second imaging system was based on a pair of NAC HiDCAM II high speed digital CMOS cameras with a resolution of 1024 x1240 pixels and a Photonics Industries GM30-5270E Nd:YLF pulsed laser. In this case the master camera TTL output pulse was used to trigger the laser

and second camera and pulse separations were selected by chosing a suitable camera frame rate. Micro Nikor 60mm lenses were used for both imaging systems.

One issue with imaging spheres of different densities was that a shadow was created by the sphere on the opposite side of the illumination. The problem was addressed by splitting the laser beam at the laser exit and generating two coaxial light sheets on either side of the sphere. This arrangement can be seen in Figure 1a where a 50/50 beam splitter is used in conjunction with a series of mirrors to direct the sheet around the tank to the opposite side of the sphere. Final alignment was achieved by observing the light sheet position relative to the centreline of the optics generating the opposite light sheet. A plano concave lens and a plano cylindrical lens were used to generate a light sheet with corresponding -55mm and 75mm focal lengths. An additional issue when viewing the spheres was reflections off the sphere surface. With these reflections, the PIV image quality was compromised adjacent to the sphere surface preventing extraction of valid PIV data. Therefore to overcome this problem, all the working fluids were seeded with fluorescent Rhodamine 6G particles and a Kodak Wratten number 21 gel filter was used to view the particles at the fluorescence wavelength of 585nm while removing any reflected 527nm or 532nm light. The particles were pre-filtered to a size range of 75µm–120µm.

Data processing was completed using ILA VidPIV software. The data processing was completed in three parts with a calibration procedure, a PIV data processing procedure and 3D data output and post-processing procedure. The calibration procedure used a set of images taken from a test grid translated through the light sheet plane. The test grid had 2.5mm diameter black dots regularly spaced on a 2.5mm square grid and 9 separate grid translations were recorded at 0, ±8, ±15, ±50 and ±100% of the sphere diameter. The PIV data processing was completed with a 16 x 16 pixel cross-correlation window with a 50% overlap. A further correlation pass was completed with an adaptive correlation and then the left and right outputs were globally filtered, interpolated and smoothed with 3 x 3 Gaussian weighted matrix before conversion to 3D data. The 3D data was further post processed by averaging series of twenty vector maps per sphere position and then overlapping sets of maps with different time delays.

Consideration of measurement error leads to the requirement for knowledge of the expected spatial velocity gradients in the flow, which will dominate in-plane error through correlation noise [Keane and Adrian (1992)]. Typically this rms error will be of the order of 0.1 pixel [Westerweel (1997)]. Thus a full scale in plane (u,v) error of 2.1% is expected from a maximum 30% particle image displacement, as recommended by Keane and Adrian (1991), when using a 16 x 16 pixel interrogation region size. The out of plane error is primarily dependent on the camera angles and given a half angle of 15^o, an out of plane (w) full-scale error of 7.8% would be expected from an error ratio of 3.7 [see Lawson and Wu (1997)].

2.3 Test Fluids and Spheres

Three different test fluids were employed in this work: a Newtonian reference fluid, a constant shear viscosity (elastic) Boger fluid, and a shear thinning elastic fluid. All three fluids have similar zero shear viscosities. The Weissenberg and Reynolds numbers were manipulated by varying both the diameter (2.38mm, 6.35mm, and 9.53mm) of the sphere and the sphere specific gravities (glass – 2.45; steel - 8.03).

For all the experiments in this paper the Weissenberg number is defined as:

$$Wi = \frac{\Psi_1\left(\dot{\gamma}\right)\dot{\gamma}}{2\eta\left(\dot{\gamma}\right)} \qquad (1)$$

where Ψ_1 is the first normal stress coefficient and $\dot{\gamma}$ is the shear rate (defined as the terminal velocity, V_t, divided by the diameter of the sphere, a). The solution shear viscosity η is a function of the shear rate. The Reynolds number is defined as

$$Re = \frac{\rho_f a V_t}{\eta_0} \qquad (2)$$

where ρ_f is the fluid density.

For the rheological study of the fluids, a TA Instruments ARES rotational rheometer with parallel plate geometry and 50mm diameter plates was used. A Peltier device attached to a re-circulating water bath was used to maintain the temperature. For the Newtonian baseline fluid, the shear viscosity was approximately 175 Pa*s. The Boger fluid had a zero shear viscosity of 30 Pa*s and a zero-shear value of the first normal stress coefficient of 9.25 Pa*s^2. For the shear-thinning fluid, the zero-shear values were η_0 = 14 Pa*s and Ψ_1 marginally greater than the Boger fluid. Further details on the fluid characteristics, including the rheological curves, are available in Tatum *et al*. (2004).

Table 1 shows the experimental conditions for the experiments described in this work.

Table 1. Test conditions for the PIV experiments performed.

Name	Diameter mm	Material	Distance From the Wall	Velocity mm/s	Shear Rate 1/s	Reynolds Number	Weissenberg Number
NF1	6.35	Glass	1	0.118	1.86E-02	1.29E-05	N/A
BF1	6.35	Glass	1	1.14	1.80E-01	7.29E-04	2.79E-02
BF2	6.35	Glass	1 / Side View	1.14	1.80E-01	7.29E-04	2.79E-02
STF4	9.53	Metal	1	83.5	8.76E+00	1.71E-01	2.05E+00

3. RESULTS AND DISCUSSION

The following section shows results from the 3D stereoscopic PIV study. The results will be presented in three sections which include the Newtonian fluid, the Boger fluid and the shear thinning fluid. Figure 1 illustrates the sign convention employed in this paper for both the position and the velocity components. The v-component of the velocity is positive in the positive y-direction (the opposite of gravity). The u-component is positive in the positive x-direction, and the w-component is positive if the fluid is flowing away from the wall or towards the center of the tank. An upward direction for the arrows on the u-w velocity vector plots corresponds to a positive w-component of velocity, i.e. fluid flowing away from the wall and in towards the center of the tank.

3.1 Newtonian Fluid

The Newtonian fluid is used as a datum as it has constant shear viscosity and is inelastic. Figures 2a and 2b show the u-v and u-w velocity vector maps for a 6.35mm glass sphere settling through a Newtonian fluid with a terminal velocity of 0.118mm/s. The sphere is dropped one ball diameter from the wall, and the laser sheet orientation is that described in Figure 1a. In Figure 2a, flow field characteristics typical of that surrounding a sedimenting sphere are clearly visible. A recirculation zone exists on either side of the sphere, and a cone-like wake extends for several diameters behind the sphere. In this case the recirculation zones are centered around x/D = ±3 and y/D = 0. The wake grows wider with increasing distance behind the sphere, extending laterally at least 2 ball diameters on either side of the sphere.

Figure 2b shows the motion perpendicular to the wall in the plane illuminated by the laser configuration shown in the Figure 1a. Because the wake extends to x/D = ±2 and the recirculation zones are centered several ball diameters from the sphere, it is expected that the presence of the wall a single ball diameter from the sphere will have a significant impact upon the flow field. This is manifested in the velocity map. In front of the sphere, the fluid is being pushed away from the wall and towards the center of the tank (in the plane of measurement). Behind the sphere, the fluid is convecting in behind the sphere as the ball drops.

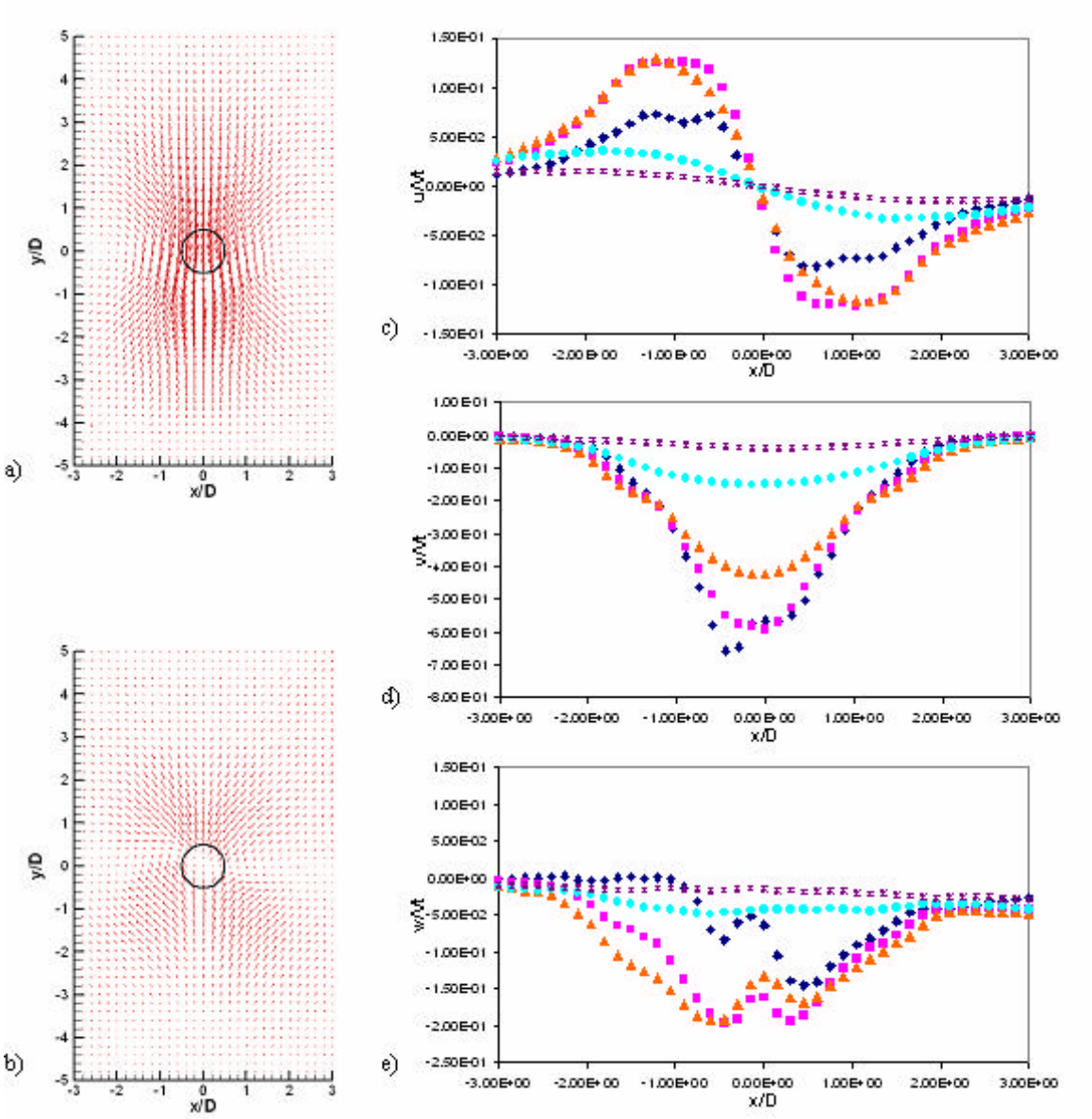

Figure 2. Data obtained for the NF1 test condition, where ◆→ y/D=0.5, ■ → y/D=1.0, ▲→ y/D=1.5, • → y/D=3.0, ∗→ y/D=4.5; a) u-v velocity vector map; b) u-w velocity vector map; c) u-component, x-direction; d) v-component, y-direction; e) w-component, z-direction.

Figures 2c-e demonstrate these flow fields in more detail by plots of the u, v and w velocity components versus x/D at various y/D planes downstream of the sphere. In Figure 2c, the peak u component of fluid velocity recorded in this experiment was around 12% of V_t at y/D = 1.0 and x/D = ±1.0. At y/D = 4.5 the presence of the recirculation zone and the wake is undetectable within experimental error.

Figure 2d indicates that the dominant velocity component in this geometry is in the direction of the sedimenting sphere. Nevertheless, the v-component of velocity decays rapidly from nearly 70% of V_t at y/D = 0.5 to around 12% of V_t at y/D = 3.0. As with the u component, the effect of the wake is virtually undetectable within the resolution of the measurement at y/D = 4.5.

As discussed above, the close proximity of the wall to the sphere leads to substantial out of plane motion away from the wall near the sphere. This is confirmed in Figure 2e, which shows the w component of velocity. The peak out of plane velocities are around 20% of V_t, which is substantially greater than the u-component. As with the other two components, the out of plane motion decays rapidly to less than 2% of V_t at y/D = 3.0 and is effectively zero at y/D = 4.5.

3.2 Boger Fluid

The Boger fluid is used to investigate the effect of elasticity in the absence of shear-thinning effects. Figure 3a shows the u-v vector map for the Boger fluid in the view that is parallel to the wall as shown in Figure 1a. This velocity vector map shows that the flow field is more localized around the sphere when compared to the Newtonian fluid. This localization of the flow leads to less interaction with the wall and thus, the w-component of velocity in this plane is negligible. There is a significant reduction in the width of the wake when compared to the Newtonian fluid, and this can be attributed to the effect of elasticity as Reynolds number in both cases is in the creeping flow regime. Thus the major difference between the scaling of the two flows is the presence of elastic forces in the Boger fluid, which retains a constant viscosity. These elastic forces act to pull the fluid vertically along with the sedimenting sphere.

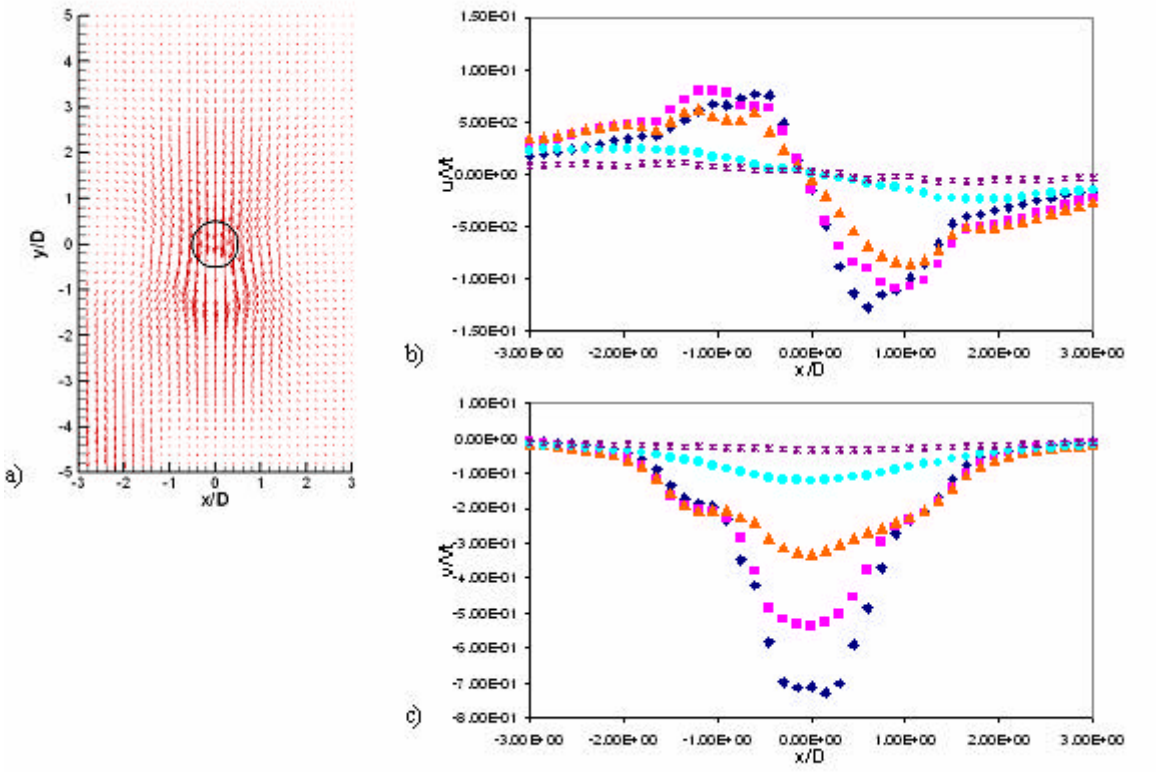

Figure 3. Data obtained for the BF1, where ◆→ y/D=0.5, ■ → y/D=1.0, ▲→ y/D=1.5, • → y/D=3.0, ∗→ y/D=4.5; a) u-v velocity vector map; b) u-component, x-direction; c) v-component, y-direction.

Figures 3b and 3c show the u and v-components of velocity (the w-component is not shown as it is negligible in the plane of measurement). These again reinforce the idea that the flow is dominated by the v-component of velocity. The maximum of the u-component is approximately 10% of V_t. This is of similar magnitude to the Newtonian fluid. Considering the v component and examining the magnitudes, it can be seen that similar maximum non-dimensional velocities exist as found in the Newtonian fluid flow with peak velocities of around 70% of V_t at y/D = 0.5 with a rapid decay of v velocity to 30% of V_t at y/D = 1.5 falling to effectively zero at x/D = 4.5. This higher v component relative to u would be expected as

the v component of velocity is dominated by viscous forces which are high in both the Newtonian and Boger fluid due to the low Reynolds number of Re < 0.001. The narrowing of the wake (relative to the Newtonian fluid) evident in Figure 3a is quantified in Figures 3b and 3c. The maximum value in the u-component occurs at x/D = ± 0.75, and drops off dramatically at x/D = ±1.5.

To further probe the impact of the wall on the flow field surrounding a sphere sedimenting near a wall, measurements were made with the laser sheet oriented perpendicular to the wall as shown in Figure 1b. The w-v velocity vector map obtained from this orientation is shown in Figure 4a. In Figure 4, z/D = -1.5 represents the wall of the tank. Figure 4a again shows that the flow is localized near the sphere with very little motion detected at z/D > 2.0.

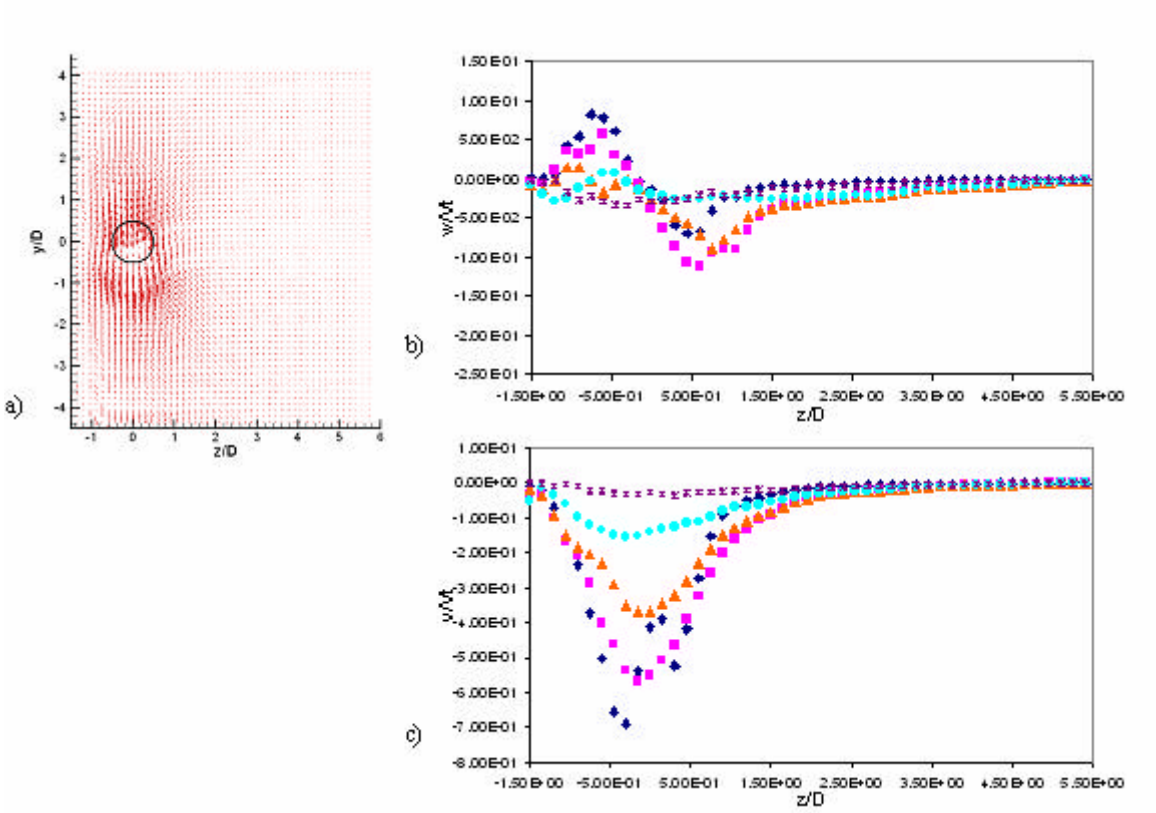

Figure 4. Data obtained for BF2, where ◆→ y/D=0.5, ■ → y/D=1.0, ▲→ y/D=1.5, • → y/D=2.5, ∗→ y/D=4.0; a) w-v velocity vector map; b) w-component, z-direction; c) v-component, y-direction.

In Figure 4a there is a recirculation zone on the open tank side of the sphere, but due to the presence of the wall no recirculation zone is present on the wall side of the sphere. The wall also appears to bias the flow almost entirely in the –y direction on the wall side of the sphere. Since the fluid between the sphere and the wall does not appear to recirculate in this region, as the sphere sediments the downstream fluid is pushed into the body of the tank and then "infills" behind the sphere. This is manifested by the arrows at y/D ~ 3 indicating the fluid behind the sphere flowing towards the wall.

Figures 4b and 4c show the w and v-components of velocity as a function of z/D at different positions behind the sphere for different y/D values. Of importance is the fact that at z/D = 0 the w-component of velocity is zero, which agrees with the data obtained from the view that is parallel to the wall. Also, due to the presence of the wall, the profiles are not symmetric around z/D = 0.

3.3 Shear-Thinning Fluid

The shear thinning fluid has a shear viscosity dependent on shear rate along with elasticity due to the added polymer. Therefore, the various fluid forces will compete to various degrees depending on the local flow conditions. This makes the shear thinning fluid the most complex of the three fluids investigated.

As shown in Figure 5a, the general trends in the fluid motion around the sphere are very similar to the Newtonian fluid. The cone-like wake grows in width with increasing distance behind the sphere. The recirculation zones are centered around x/D = ±2, and there is a significant u-component of the velocity. One important characteristic of the shear-thinning fluid for the sedimenting sphere is the formation of negative wakes in experiments where the sphere is dropped along the centerline of a cylindrical tank [Arigo and McKinley (1998). For the first time, we report the existence of negative wakes when the sphere is dropped adjacent to a vertical wall. The negative wake was found to appear only at high Weissenberg numbers (> 1.7). The experiment shown in Figure 5 represents a Weissenberg number of 2.05.

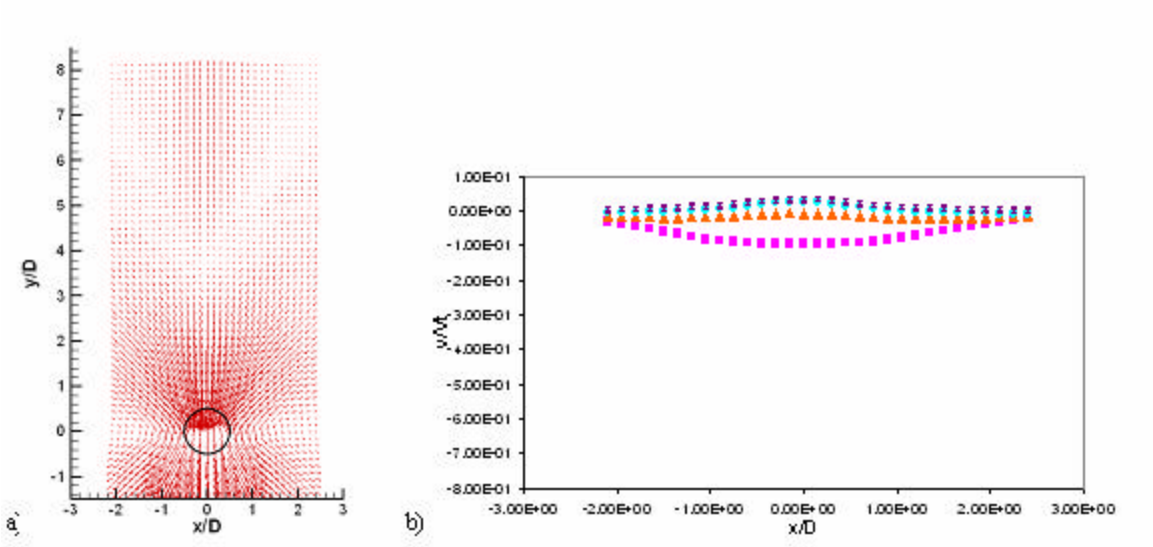

Figure 5. Data obtained for the STF4 test condition, where ■ → y/D=2.0, ▲→ y/D=3.5, • → y/D=5.0, ∗→ y/D=8.0; a) u-v velocity vector map; b) v-component, y-direction.

The negative wake can be seen to start at about y/D = 3.8. The magnitude of the negative wake is very small when compared to the settling velocity of the sphere, as shown in Figure 5b. Figure 5 also shows that as the distance behind the sphere increases, the width of the negative wake increases, although the greatest values of the velocity are along the x/D = 0 axis behind the sphere.

4. CONCLUSION

This work has presented an angular stereoscopic PIV study of the three-dimensional flow field generated by a sphere sedimenting one diameter from a wall in both Newtonian and non-Newtonian fluids. This flow presents a challenging test case in non-Newtonian fluid mechanics for numerical modelers. Data was recorded from planes of interest about the centerline of the sphere both parallel to and perpendicular to the wall. The test fluids included a Boger fluid to isolate the effects of elasticity, a shear thinning fluid to investigate the competing shear thinning and elastic effects and a Newtonian datum fluid for comparison with the non-Newtonian fluids.

The isolated effects of adding elasticity to a Newtonian fluid are observed in the Boger fluid. The most prominent difference is the reduction in the width of the wake behind the sphere. A consequence of the reduction of the wake width was found to be a reduction in the maximum out of plane velocities (i.e. perpendicular to the wall) from 20% in the Newtonian test case to less than 5% in the Boger fluid. Further

studies of the Boger fluid flow field in a plane perpendicular to the confirmed these flow characteristics, and also demonstrated the effects of the wall. The presence of the wall leads to the loss of the recirculation zone on the wall side of the tank, and consequently the fluid "infills" behind the sphere from the center of the tank leading to motion towards the wall

Velocity data from the shear thinning fluid flow characteristics similar to that of the Newtonian fluid. These trends are attributable to the competing effects of fluid elasticity as well as the local reductions in viscosity adjacent to the sphere due to the shear-thinning nature of the fluid. In addition, a negative wake was observed that originated at a distance of y/D = 3.8.

ACKNOWLEDGMENT

This material is based upon work supported by the National Science Foundation under Grant No. INT-0309459.

REFERENCES

Adrian R. J., Particle-imaging techniques for experimental fluid-mechanics, Ann. Rev. Fluid Mech., 23 (1991) 261.

Arigo M. T. and McKinley G. H., An experimental investigation of negative wakes behind spheres settling in a shear-thinning viscoelastic fluid, Rheologica Acta, 37 (1998) 307.

Becker L. E., McKinley G. H., and Stone H. A., Sedimentation of a sphere near a plane wall: weak non-Newtonian and inertial effects, J. of Non-Newtonian Fluid Mech., 63 (1996) 201.

Bush M. B., The stagnation flow behind a sphere, J. of Non-Newtonian Fluid Mech., 49 (1993) 103.

Bush M. B., On the stagnation flow behind a sphere in a shear-thinning viscoelastic liquid, J. of Non-Newtonian Fluid Mech., 55 (1994) 229.

Chhabra R. P., Uhlherr P. H. T., and Boger D. V., The influence of fluid elasticity on the drag coefficient for creeping flow around a sphere, J. of Non-Newtonian Fluid Mech., 6 (1980) 187.

Chmielowski C., Nichols K. L., and Jayaraman K., A comparison of the drag coefficients of spheres translating in corn-syrup-based and polybutene-based Boger fluids, J. of Non-Newtonian Fluid Mech., 35 (1990) 37.

Harrison G. M., Lawson N. J., and Boger D. V., The measurement of the flow around a sphere settling in a rectangular box using 3-dimensional particle image velocimetry, Chem. Eng. Comm., 188 (2001) 143.

Hassager O., Working group on numerical techniques, J. of Non-Newtonian Fluid Mech., 29 (1988)

Joseph D. D., Liu Y. J., Poletto M. and Feng J., Aggregation and dispersion of spheres falling in viscoelastic liquids, J. of Non-Newtonian Fluid Mech., 54 (1994) 45.

R. Keane and R. J. Adrian, Theory of cross-correlation analysis of PIV images, J. of Applied Sci. Res., 49 (1992) 191.

Lawson N.J., Wu J. Three-dimensional particle image velocimetry: experimental error analysis of a digital angular stereoscopic system. Meas Sci Technol 1997;8:1455-64

Mena B., Manero O., and Leal L. G., The influence of rheological properties on the slow flow past spheres, J. of Non-Newtonian Fluid Mech., 26 (1987) 247.

Prasad A.K. “Stereoscopic Particle Image Velocimetry”, Exp. in Fluids 29(2), p103-116, (2000)

Prasad K. and Jensen K., Scheimpflug stereocamera for particle image velocimetry in liquid flows, Applied Optics, 34 (1995) 7092.

Sigli D. and Coutanceau M., Effect of finite boundaries on the slow laminar isothermal flow of a viscoelastic fluid around a spherical obstacle, J. of Non-Newtonian Fluid Mech., 2 (1977) 1.

Singh P. and Joseph D. D., Sedimentation of a sphere near a vertical wall in an Oldroyd-B fluid, J. of Non-Newtonian Fluid Mech., 94 (2000) 179.

Tanner R. I., End effects in falling-ball viscometer, J. of Fluid Mech., 17 (1963) 161.

Tatum J.A., Finnis M.V., Lawson N.J, Harrison G.M. 3-D Particle Image Velocimetry of the Flow Field Around a Sphere Sedimenting Near a Wall. Part 1. Effects of Weissenberg Number. submitted to Journal of non-Newtonian Fluid Mechanics, March 2003.

Westerweel, J. Fundamentals of digital particle image velocimetry. Measurement Science Technology, 1997, 8, 1379